International Journal of Applied Engineering Research, ISSN 0973-4562 Vol. 10 No.20 (2015)

Efficient Hybridized framework for Denoising of Images using TIDFT with Gabor filters and BM3D

N.Kalyani[1]
[#1]ME (Communication & Networking) Scholar (II Year),
Cape Institute of Technology,
Levengipuram, Tirunelveli.
duraikalyani91@gmail.com

A.Velayudham[2]
[#2]Assistant Professor (Selection Grade) / Department of Information Technology,
Cape Institute of Technology, Levengipuram, Tirunelveli.
sunilvel@gmail.com

***Abstract*— In this research work, it has been proposed to denoise natural and medical images employing Translation Invariant Directional Framelet Transform (TIDFT). In this paper, emphasis is on removing noise in natural and medical images of various sized dimensions. TIDFT is able to find singularities in a given direction set, along with this orientation estimation method based on Gabor filter is introduced instead of the conventional approach, wherein vertical horizontal lifting has been employed. BM3D is a recent denoising method is added for denoising an image. In extension, TIDFT has utilized an MAP estimator which supports two noise reduction methods which comes under distribution function. Finally the obtained denoising results using TIDFT and BM3D are compared with other transforms such as (TIADL, NSCT, DST) to identify the denoising potential. The performance parameters PSNR and SSIM have been taken into account and the noise is reduced from original signal.**

***Index Terms*— Denoising images, Directional Framelet, Gabor Filter, MAP estimator.**

I.INTRODUCTION

In the Past decades it has been widely discussed about the directionality in the wavelet or sub band based transform. Two well-known tools such as *Curvelets* [1] and *contourlets* [2] are used for capturing the directional information. Curvelets, develop a transform in the continuous domain and then discrete for sampled data. We start it with a discrete-domain construction and then read it convergence to an expansion in the continuous domain. In counterlet we construct a discrete-domain, multiresolution and multidirection. Apart from curvelets and contourlets, many other directional transforms have been proposed, such as *ridgelets [3]*, bandelets [4], *dual-tree complex wavelets* [5], *shearlets* and *directional filter banks* [6]. Now recently, the adaptive directional lifting (ADL) transform has been rapidly developing [7]. It is different from the conventional 2-D lifting transform and then it also applicable in the predicted direction as well as horizontal/vertical ones. Finally it gives an efficient representation for images containing rich orientation features. By the motivation of existing works, we are devoted to studying the adaptive directional lifting transform for wavelet frames. Researchers who have proposed these kinds of improved methods for image processing [8]. In our previous works the lifting factorization theorems of wavelet frames, which have been developed [9]–[11], to provide general principles to construct wavelet frames through lifting. However, in our previous works neither the directionality nor the translation invariance has been involved. In this paper, it has been proposed to denoise natural images employing Translation Invariant Directional Framelet Transform (TIDFT). In extension of the conventional lifting scheme, the translation invariant structure provides a redundant representation which has been proved to be substantially superior to a non-redundant representation for image denoising [12]. Add to that, we propose orientation estimation based on Gabor filters, instead of the conventional approach. Conventional orientation estimation it is effective for uncorrupted images but does not work well within corrupted images.In fact, the features of local image may be disturbed by the noise. Different approaches have been developed by number of researchers to modeling the coefficients in wavelet domain, including hidden Markov model [13],generalized Gaussian [14], Gaussian scale mixture [15], Laplacian and its variations [16], and exponential distribution [17] etc. Thus the MAP estimator which introduce two Noise Reduction method for denoise an image ie; spherically contoured exponential (SCE) and elliptically contoured exponential (ECE) distributions [17] to exploit the dependencies of inter-scale and intra-scale. With the MAP estimator, we can also derive two data-driven estimation methods for denoising.

Overall, the contributions of this paper have three aspects:

1. A translation invariant directional lifting scheme for wavelet frames.
2. An adaptive and robust orientation estimation based on discrete Gabor filter

3. Two noise reduction methods using MAP estimator to exploit the inter-scale and intra-scale dependencies of framelet coefficients.

II. TRANSLATION INVARIANT LIFTING SCHEME

The lifting scheme is not translation invariant since the Lifting procedure involves sub sampling. In image denoising and pattern recognition, translation invariance is a desirable property in many applications. Translation invariance can be achieved through different ways.

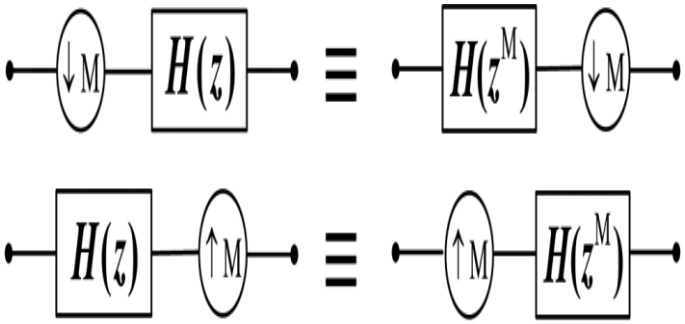

Fig.1.Multirate identify for interchange of sub sampling and filtering.

The authors used the cycle-spinning algorithm which was originally developed [18] for denoising. [19] Provided an over complete lifting scheme by using a smoothing *Lazy* wavelet in the split stage which does not subsample but smooth the input image. On the other hand, the most commonly used approach to achieve translation invariance is removing the down samplers and up samplers and up sampling the filter coefficients by a factor of 2^{l-1} in the *l*-level of the transform, so called *algorithme à trous* [20]. And a generalized version for multidimensional filter banks refers to [21].

According to the multirate identity (see Fig.1), down sampling followed by filtering with *H (z)* is equivalent to filtering with H (*zm*) followed by down sampling, where *M* is an integer number. Thus it is straightforward to omit the sub sampling operation in the traditional lifting scheme by up sampling the polyphase matrix **P** *(z).*

III. TRANSLATION INVARIANT DIRECTIONAL FRAMELET TRANSFORM

In this section, we shall discuss the directional lifting structure of wavelet frames. It can be much more directionally selective for image processing than orthogonal or biorthogonal wavelets. It can also be shift invariant whereas an orthogonal or biorthogonal wavelet transform is not shift invariant wavelet frames are less sensitive to corruption of coefficients.

.

A. Translation Invariant Directional Lifting Structure

Consider a 2-D signal $x(\mathbf{n})$, $\mathbf{n} = [m, n]$ where m, n denote the index of row/column respectively.

.

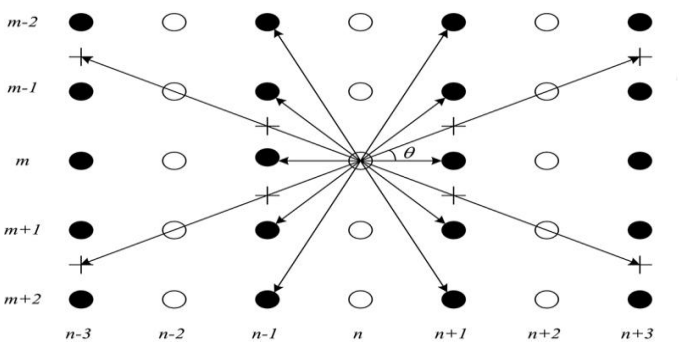

Fig .2.Directions used in the propose TIDFT, where the integral pixels '•'s and the fractional pixels '+'s are used for prediction'◦' s.

We assume that the 1-D transform is first applied in the horizontal direction and then in the vertical direction without a loss in generality. Assume that $\mathbf{P}(z)$ can be factorized into one couple of lifting steps, In this paper, seven directions as depicted in Fig.2 is preassigned to take part in the prediction step as well as in the update step .It is reasonable to expect that the transform will benefit from more directions used. Since the noise can deteriorate the estimation accuracy it is not feasible for a corrupted image. In extensions, the performance gain is limited with increasing directions. It will be further verified through experimental results in Section VI.

B. Tight Frame TIDFT

This tight frame is generated by a *B*-spline refinable function and two framelets with vanishing moments of order 2 and 1 respectively [22]. The constant signals cannot pass through the high-pass filter h_2 but it can pass through h1,while linear signals can also pass through h_1. Thus h_1, h_2 can be considered as singular detectors of order two and one respectively. For large numbers of natural images, these two framelets are capable of capturing the essential texture information since the natural images are often piecewise smooth and locally auto correlated. Thus this tight frame provides a sparse approximation to piecewise smooth images.

IV. ORIENTATION ESTIMATION BASED ON GABOR FILTER

A. Discrete Gabor Filters Construction

The Gabor function is frequently used in image processing due to the well noise-insensitiveness capability and spatial locality [23]–[25]. Here we consider the real part of the Gabor function defined as

$$g_{R(x,y)} = h(x', y') \quad (1)$$

Where $x = x\cos\theta + y\sin\theta$, $y = -x\sin\theta + y\cos\theta$, F is the

spatial frequency of the sinusoidal wave plane, and *h(x, y)* is the Gaussian function, A typical Gabor analysis is usually time-consuming. But in this paper we propose a construction of discrete Gabor filter that effectively extract the orientation information. The spatial frequency *F* is also a key parameter that determines the shape of the function. In this paper we applied one single *F* by using the orientation information based on the fine details of high frequencies. For the computational efficiency, we assume that the wavelength of the sinusoid equals to half the diagonal length of the rectangle encapsulates the Gaussian envelope.

B. Select Orientation and Examine Robustness

Note that the oscillation resulting from the sinusoid is along the direction θ. Apparently the edges perpendicular to the direction produce strong responses as the gray level intensity changes abruptly, whereas the edges along the same direction respond mildly as the intensity is nearly the same. Here the direction is selected in block-wise fashion but filtering in the prediction and update step extends across block boundaries. So that the blocking artifacts are not produced in the reconstruction.

Hence we demonstrate the orientation estimation results in Fig.3 for two corrupted images "*Barbara*" and "*Monarch*" with different standard deviation of noise, compared to the methods ROE [8] which is based on the minimization of the residuals, and the Gabor approach adopted (denoted as GF). The orientation accuracy estimated by the ROE decreases with the increasing standard deviation of noise. Due to the pixel-wise implementation the GF provides 16 directions, as recommended by the authors, to increase the estimation accuracy, the estimation tends to be irregular in the texture region with increasing standard deviation of noise.

TABLE I
DIRECTION GAIN. THE NUMBER IN BRACKETS IS THE NUMBER OF DIRECTIONS

σ	Ver/Hor (2)	ROE (7)	GABOR (7)	GABOR (9)	GF (16)
10	6.35	7.82	10.78	11.31	9.36
20	3.60	4.95	6.56	6.72	5.24
30	2.52	2.78	4.27	4.55	3.67
40	1.91	2.14	3.42	3.59	2.95
50	1.54	1.75	2.82	2.79	2.27

On the other side, benefitting the block-wise strategy, the estimation proposed in this paper can capture the orientation information in a robust way. Since the MSE distortion is proportional to the geometric mean of the sub band variances, The directional adaption gain can be evaluated by the variances [7]. For the low-pass sub band, large variance implies that the filtered image contains rich textures. Thus most energy is preserved in this sub band while other sub bands can be coded in few bits. However, this is not always true for corrupted images since the noise may dominate the variance.

One level TIDFT combining with the Gabor estimation is carried out with a numbers of images corrupted by different noisy level. In this concept the ROE and GF are compared. Besides, the conventional framelet, i.e., horizontal/ vertical lifting and more direction candidates up to 9 are also included to compare the direction gain. To make the evaluation more compact we average the results of each image and illustrate them in Table I.

As shown in Table I, the entire values decline with increasing noise level, which means that the noises at larger level occupy more energy in the low-pass sub band. Both the ROE and Gabor which shows the capability of capturing the texture information. Where the ROE is based on the minimization of residuals, the noises are also transformed into low-pass sub band. By using Gabor filters it can also balance the noise-eliminating and edge-preserving well. Thus the gain is superior to the ROE. It is also a proven fact that the GF is less efficient than the proposed method due to the redundant implementation. In addition the result of using 9 directions is slightly better than 7 directions. However the improvement is not significant. Therefore 7 directions are sufficient to capture the orientation information in the prediction.

C. Complex TIDFT Combined With Gabor Filters

At the end of this section, we take a look at the computational complexity of the proposed TIDFT. Here we assume input image size as N. In the orientation estimation step, filtering the image with Gabor filter whose size of mask is $L \times M$ takes LM multiplications and $LM - 1$ additions. We consider the maximum consumption, i.e., the estimation proceeds in pixel-wise fashion, though in practice the block-wise processing will further speed the implementation. Thus the orientation estimation takes $K(2LM - 1)$ operations at each pixel, where K is the number of the directions.

In the lifting step, a couple of prediction and update takes 6 additions and 6 multiplications plus one interpolation (simply average) for the fractional pixel. So the total number is up to 14 for one pixel. Since the TIDFT produces three sub bands whose size is equal to the original after one separable lifting transform, the total number of operations for one complete lifting is $14 \times 4N$. Combined with the orientation estimation, the number of operations for one-level TIDFT transform is $N(2KLM - K + 56)$. For l-level transform the operation is up to l times the consumption of one-level transform since the transform is non-subsampled.

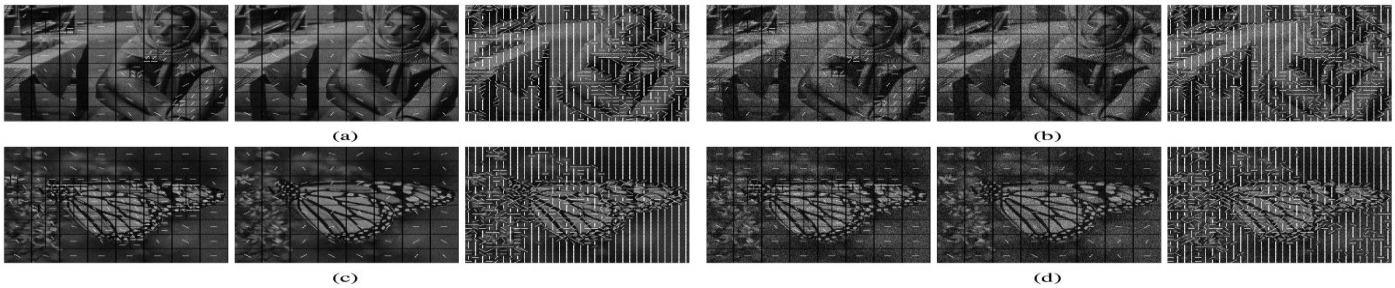

Fig.3. Orientation estimation for the noisy images "*Barbara*" and "*Monarch*", (a) σ = 20, (b) σ = 50, (c) σ = 20, (d) σ = 50. From left to right: the proposed method, ROE, GF

IV. BM3D GRAYSCALE IMAGE DENOISING

BM3D is a recent denoising method based on the fact that an image has a locally sparse representation in transform domain. A noisy (σ = 25) House image and the corresponding BM3D estimate. In this test image, similarity among neighboring blocks is easy to perceive in the uniform regions and along the regular-shaped structures. Hence, such details are well-preserved in the estimate. The denoising performance of the BM3D algorithm is further illustrated where we show fragments of a few noisy (σ = 25) test images and fragments of the corresponding denoised ones. The denoised images show good preservation of:

- uniform areas and smooth intensity transitions (cheeks of Lena, and the backgrounds of the other images),
- textures and repeating patterns (the scarf in Barbara),

A denoising example for an extreme level of noise such as σ = 100. Given that the original image is almost completely buried into noise, the produced estimate shows reasonable detail preservation. In particular, repeated patterns such as the stripes on the clothes are faithfully reconstructed. Regarding the subjective visual quality, we and that various image details are well preserved and at the same time very few artifacts are introduced. The state-of-the-art subjective visual quality of our algorithm is confirmed by the result of the psycho-visual experiment carried out by Vansteenkiste. There, 35 evaluators classified the preliminary version of the BM3D algorithm as the best among 8 evaluated state-of-the art techniques. The criteria in this evaluation were perceived noisiness, perceived blurriness, and overall visual quality. Furthermore, we consider the subjective visual quality of the current BM3D algorithm to be significantly better (in terms of detail preservation) than that of its preliminary version evaluated. Which show images denoised by the current and by the preliminary versions of the BM3D algorithm. A close inspection reveals that the images denoised by the current BM3D have both fewer ringing artifacts and better preservation of details. We show the PSNR performance of the Fast and Normal BM3D. Graph at about σ = 40 due to erroneous grouping. On the other hand, for the σ > 40. graph, where the thresholding-based d-distance is used with a relatively large block-size N1, one can observe that there is no sharp PSNR drop. It is noteworthy that for up to moderate levels of noise, such as σ < 35, the PSNR difference between the Fast and the Normal is in the range 0.05. This can be an acceptable price for the 6-fold reduction of the execution time shows more precisely, the approximate execution time (for denoising a 256*256 image calculated on a 1.5 GHz Celeron decreases from 4.1 seconds for the Normal to 0.7seconds. The BM3D algorithm allows for further complexity/performance trade-off by varying N step. As a rough comparison, the execution times (for denoising a 256*256 image on a 1.5GHz Celeron M) of the other methods were: 22.1 seconds for the BLS-GSM, 6.2 seconds for the SA-DCT 9. 30 minutes depending on for training the adaptive K-SVD on an input noisy image and 25 .120 seconds to perform the altering using the found dictionary. The execution time of the exampler-based method was reported in to be about 1 minute when measured on a 2 GHz Pentium IV. The execution time of the FSP+TUP BLSGSM was not reported; however, it is a two-step BLS-GSM extension that should not be faster than BLS-GSM.

V. DENOISING IMAGES USING THE TIDFT AND BM3D

In the rest of this paper, we shall utilize the proposed TIDFT to exploit the capability of image denoising.

A. MAP Estimator of SCE and ECE Models based Noise Reduction

Let **y** denote a group of the framelet coefficients corrupted by the Gaussian white noise,

$$\mathbf{y} = \mathbf{s} + \mathbf{n}, \qquad (2)$$

Where x is the original signal, **n** is a *d*-dimensional zero-mean Gaussian random vector. Here we consider both the inter-scale and intra-scale dependencies. It has been proved that the coefficients in wavelet domain features non-Gaussian [14]–[16]. Though the distribution of framelet coefficients also inherits the behaviors that are peaked, long-tailed and approximately symmetric we introduce the spherically contoured exponential (SCE) distribution [17] to further

TABLE II
COMPARISON OF TIME CONSUMPTION (sec)

IMAGE SIZE	TIADL	TIDFT(SCE)	DST	NSCT	TIDFT(ECE)	BLS-GSM	BM3D
1024*1024	10.4	16.1	32.1	131.5	26.2	64.6	19.5
512*512	3.2	5.0	9.3	32.1	9.7	20.7	3.9
256*256	1.4	1.5	1.6	8.5	1.9	7.5	0.8

exploit the dependency between scales, we introduce the elliptically contoured exponential distribution [17].

B. Denoising Results

It includes four gray level images "*Lena*", "*Barbara*", "*Monarch*", "*Goldhill*" to verify the denoising potential of the proposed TIDFT. The noise experiment consists of two groups. In the first group, we here to examine the sparse representation capability of the TIDFT which is compared to the translation invariant directional lifting (*TIADL*) which adopts the 9/7 kernel for transform, the nonsubsampled contourlet transform (*NSCT)* and the discrete shearlet transform (*DST*) [7]. Above mentioned transforms runs over 4-level decomposition and use the same shrinkage. In the second group, to further exploit the denoising potential of the TIDFT, we use the estimation based on ECE model. In extensions, two well-known approaches such as BL-GSM [15] and BM3D are included for comparison.

To show the computational complexity, we provide the average time consumptions in TableII. TIADL takes the least running time, followed by the BM3D, since the TIADL is a wavelet-based denoising method. Among the frame-based transforms, the TIDFT takes the least time compared to the NSCT and DST. Here by using the iterative estimation will increase the computation (ECE versus SCE), the expense is moderate. Due to its redundant transform and sophisticated estimation the BLS-GSM is time-consuming. Definitely, the TIDFT has an advantage over the other frame-based methods in computational complexity.

For the denoising performance, the comparison of PSNR is illustrated in Table III. As shown in Table III, the TIDFT (SCE) is significantly superior to the TIADL with gains of 1 dB or more. Compared to the other frame-based transforms our TIDFT (SCE) yields better results than NSCT and DST. For the image *Barbara* that contains large amount of texture, the TIDFT (SCE) and DST produce very similar results, even better than BLSGSM, which proves that the TIDFT can achieve an efficient sparse representation. Furthermore, using the iterative estimation based on ECE model does improve the results with gains of 0.3 dB around, especially for $\sigma \leq 50$. However for a large σ, the gain of ECE is marginal or even inferior to SCE in some cases like *Goldhill*, .In the group two, the BM3D which exhibited excellent noise reduction performance in most cases.

Three key points which shows why the TIDFT (ECE) is slightly less efficient than the BM3D. Firstly the BM3D runs over the 3-D overlapping data, rather than the 2-D pixels, which provides more redundancy for estimation. Secondly the estimation adopted in the TIDFT is based on the MAP estimator whereas the BM3D uses the Wiener filtering derived from the minimum mean square error (MMSE) estimator. Theoretically the MMSE can achieve the best results [16]. However, for the SCE and ECE models, one of the disadvantages of using MMSE estimator is the complex and lengthy computations, which has been demonstrated in [17]. Thus we consider the MAP as a good substitute for the MMSE. Lastly the BM3D incorporates two step estimation which further improves the quality of noise reduction. In most cases, the TIDFT (ECE) performs better than the BLS-GSM. It is also noted that there exist the BLS-GSM two key distinctions between them. Firstly the TIDFT proposed in this paper, compared to the steerable pyramid transform [15] used In BLS-GSM, has advantages on local directional adaptiveness and fast implementation. Benefitting from the directionality and translation invariance, the TIDFT can achieve sparse representation while not producing aliasing. Secondly, as opposed to the Bayes least squares (BLS) estimator, the MAP estimator does not require numerical integration. This is why the TIDFT took much less time than the BLS-GSM as shown in Table II. In addition, the TIDFT (SCE) also produces pleasant results though slightly loss in PSNR. Since the MAP incorporating with SCE derives a closed-form shrinkage function, which is quite desirable in shrinkage-based denoising, we believe that the TIDFT is details when σ is large. Very pleasant results is yielded by TIDFT (ECE) and BM3D yield.

TABLE III

COMPARISON OF PSNR (dB) FOR VARIOUS NATURAL IMAGES AND σ VALUES

Group I					Group II				
Image	**σ**	**noisy**	**TIADL**	**NSCT**	**DST**	**TIDFT (SCE)**	**TIDFT (ECE)**	**BLS- GSM**	**BM3D**
Lena (512*512)	10	28.13	35.09	35.34	35.60	36.14	36.20	36.12	36.43
	20	22.14	31.85	32.16	32.40	32.72	32.98	33.10	33.12
	30	18.66	30.01	30.15	30.44	31.09	31.24	31.37	31.26
	40	16.30	28.24	28.54	28.76	29.67	29.80	29.87	29.85
	50	14.54	27.44	27.65	27.94	28.43	28.71	28.56	29.19
	75	11.74	24.61	25.21	25.38	25.90	26.11	25.34	26.36
	100	10.11	22.85	23.10	23.08	23.48	23.78	22.93	24.17
Barbara (512*512)	10	28.13	32.16	33.54	33.68	33.64	33.81	34.04	34.71
	20	22.14	28.89	29.45	29.98	30.04	30.37	30.34	31.40
	30	18.66	26.71	27.55	27.83	27.86	28.01	27.69	29.32
	40	16.47	24.77	26.07	26.26	26.25	26.54	26.10	27.80
	50	14.76	23.36	24.32	24.94	25.00	25.23	24.29	26.64
	75	11.92	21.38	22.11	22.32	22.07	22.55	21.67	23.68
	100	10.25	20.35	20.43	20.46	20.04	20.43	20.03	21.24
Monarch (512*512)	10	28.13	33.31	34.69	34.41	35.06	35.21	35.04	35.75
	20	22.14	29.69	31.07	30.56	31.55	31.71	31.58	31.95
	30	18.71	27.75	28.14	28.69	29.34	29.77	29.50	29.81
	40	16.37	26.28	27.54	27.15	27.88	28.20	27.71	27.98
	50	14.66	24.83	26.34	26.02	27.03	27.22	26.10	27.16
	75	11.85	22.41	23.28	23.50	24.09	24.15	22.81	24.30
	100	10.20	19.98	20.99	21.06	21.32	21.25	20.46	22.02
Goldhill (512*512)	10	28.13	32.46	32.80	32.94	33.15	33.21	33.58	33.55
	20	22.17	29.46	29.91	29.73	30.09	30.21	30.19	30.55
	30	18.75	27.77	28.04	27.87	28.30	28.50	28.35	28.88
	40	16.42	26.62	26.95	26.74	27.08	27.40	27.37	27.55
	50	14.68	25.49	25.80	25.81	26.11	26.45	26.24	26.75
	75	11.85	23.39	23.73	23.77	24.05	23.96	23.78	24.63
	100	10.19	21.17	21.75	22.01	21.97	21.83	21.76	22.67

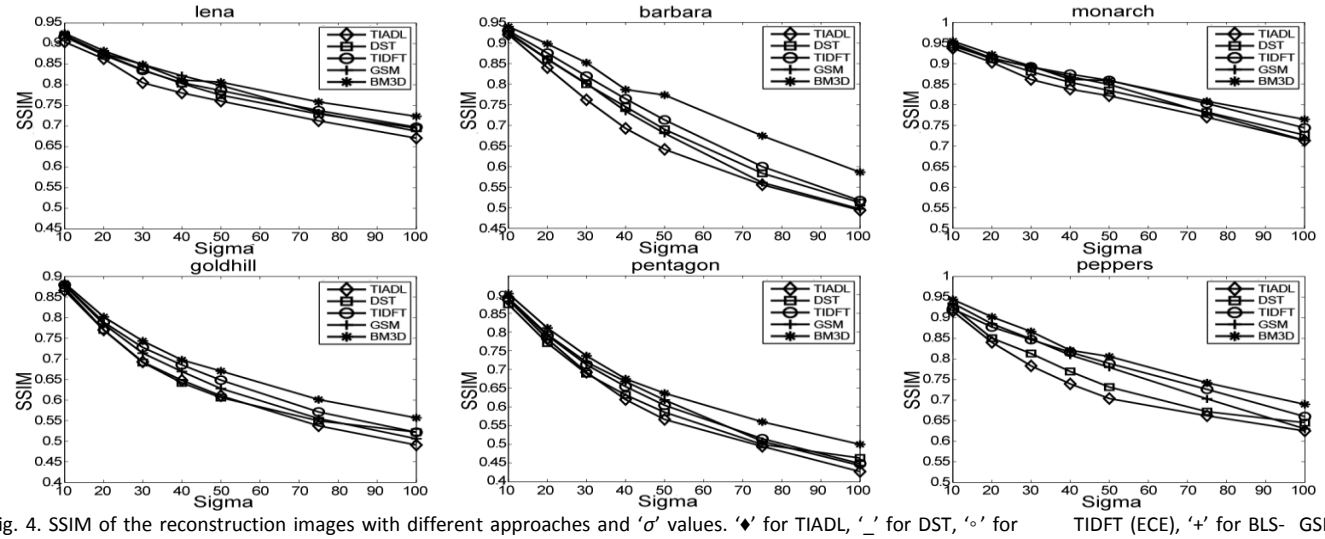

Fig. 4. SSIM of the reconstruction images with different approaches and 'σ' values. '♦' for TIADL, '_' for DST, '◦' for TIDFT (ECE), '+' for BLS- GSM and '∗'forBM3D

TABLE IV

COMPARISON OF PSNR (dB) FOR VARIOUS MEDICAL IMAGES AND σ VALUES

Group I					Group II				
Image	**σ**	**noisy**	**TIADL**	**NSCT**	**DST**	**TIDFT (SCE)**	**TIDFT (ECE)**	**BLS- GSM**	**BM3D**
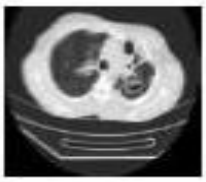	10	30.13	36.09	36.34	36.60	37.14	37.20	36.12	39.43
	20	24.14	32.85	33.16	33.40	33.72	33.98	33.10	35.12
	30	20.66	31.01	31.15	31.44	32.09	32.24	31.37	33.26
	40	18.30	29.24	29.54	29.76	30.67	30.80	29.87	31.85
	50	14.54	28.44	28.65	28.94	29.43	29.71	28.56	31.19
	75	13.74	25.61	26.21	26.38	26.90	27.11	25.34	28.36
	100	12.11	23.85	24.10	24.08	24.48	24.78	22.93	26.17
	10	30.13	33.16	34.54	34.68	34.64	34.81	34.04	36.71
	20	24.14	29.89	30.45	30.98	31.04	31.37	30.34	33.40
	30	20.66	27.71	28.55	28.83	28.86	29.01	27.69	32.32
	40	18.47	25.77	27.07	27.26	27.25	27.54	26.10	30.80
	50	16.76	24.36	25.32	25.94	26.00	26.23	24.29	28.64
	75	13.92	22.38	23.11	23.32	23.07	23.55	21.67	25.68
	100	12.25	21.35	21.43	21.46	21.04	21.43	20.03	23.24
	10	30.13	34.31	35.69	35.41	36.06	36.21	35.04	38.75
	20	24.14	30.69	32.07	31.56	32.55	32.71	31.58	33.95
	30	20.71	28.75	29.14	29.69	30.34	30.77	29.50	31.81
	40	18.37	27.28	28.54	28.15	28.88	29.20	27.71	29.98
	50	16.66	25.83	27.34	27.02	28.03	28.22	26.10	29.16
	75	13.85	23.41	24.28	24.50	25.09	25.15	22.81	28.30
	100	12.20	20.98	21.99	22.06	23.32	22.25	20.46	26.02
	10	30.13	33.46	33.80	33.94	34.15	34.21	33.58	33.55
	20	24.17	30.46	30.91	30.73	31.09	31.21	30.19	33.55
	30	20.75	28.77	31.04	28.87	29.30	29.50	28.35	30.88
	40	18.42	27.62	27.95	27.74	28.08	28.40	27.37	29.55
	50	16.68	28.49	26.80	26.81	27.11	27.45	26.24	28.75
	75	13.85	24.39	24.73	24.77	25.05	24.96	23.78	26.63
	100	12.19	22.17	22.75	23.01	22.97	22.83	21.76	24.67

Fig. 5. Details of the denoising images, σ = 40 (a)*lena*, (b)*Barbara*, From left to right: TIADL, DST,TIDFT (ECE), BLS-GSM and BM3D

The output PSNR results of the BM3D algorithm for a standard set of grayscale images are given in Table IV. For σ =10 the First image which gives PSNR value 37.20 for TIDFT and 39.43 for BM3D.Then the second image which gives PSNR value 31.37 for TIDFT and 33.40 for BM3D when σ =20.And the third image which gives PSNR value 30.77 for TIDFT and31.81 for BM3D when σ =30. the Fourth image which gives PSNR value 28.40 for TIDFT and 29.55 for BM3D when σ=40.Hence our BM3D which shows better PSNR values compared to TIDFT. The main purpose for denoising of is to improve image quality.

VI. CONCLUSION

In this paper we have presented a translation invariant lifting structure for wavelet frames. We also proposed a specific translation invariant directional framelet transform (TIDFT) incorporated, with a novel orientation estimation based on Gabor filters. In addition, the TIDFT utilized MAP estimator for denoising. Since the TIDFT denoising method which provides better texture preserving than other transform such as contourlet and shearlet. It is consider as a superior frame based transform. Compared to the state-of-the-art methods like BLS-GSM and TIADL, DST our proposed method yielded similar or even better results along with low computational complexity and robust implementation. Consequently the TIDFT can be regarded as a competent approximation tool for image denoising.

Besides, benefitting from the translation invariance, the TIDFT can also be applied to other applications such as image fusion and feature extraction since the redundancy is helpful. In addition, higher dimensional directional transforms have been studied recently, such as surfacelets ,3D curvelets and BM3D.

REFERENCES

[1] E. J. Candes and D. L. Donoho, "Curvelets: A surprisingly effective nonadaptive representation of objects with edges," in *Curves and Surface Fitting: Saint-Malo*, A. Cohen, C. Rabut, and L. L. Schumaker, Eds. Nashville, TN, USA: Vanderbilt Univ. Press, 2000.

[2] M. N. Do and M. Vetterli, "The contourlet transform: An efficient directional multiresolution image representation," *IEEE Trans. Image Process.*, vol. 14, no. 12, pp. 2091–2106, Dec. 2005.

[3] M. N. Do and M. Vetterli, "The finite ridgelet transform for image representation," *IEEE Trans. Image Process.*, vol. 12, no. 1, pp. 16–28, Jan. 2003.

[4] E. L. Pennec and S. Mallat, "Sparse geometric image representations with bandelets," *IEEE Trans. Image Process.*, vol. 14, no. 4, pp. 423–438, Apr. 2005.

[5] I. W. Selesnick, R. G. Baraniuk, and N. Kingsbury, "The dual-tree complex wavelet transforms—A coherent framework for multiscale signal and image processing," *IEEE Signal Process. Mag.*, vol. 22, no. 6, pp. 123–151, Apr. 2005.

[6] T. T. Nguyen and S. Oraintara, "Multiresolution direction filterbanks: Theory, design, and applications," *IEEE Trans. Image Process.*, vol. 53, no. 10, pp. 3895–3905, Oct. 2005.

[7] C. L. Chang and B. Girod, "Direction-adaptive discrete wavelet transform for image compression," *IEEE Trans. Image Process.*, vol. 16, no. 5, pp. 1289–1302, May 2007.

[8] X. Wang, G. Shi, Y. Niu, and L. Zhang, "Robust adaptive directional lifting wavelet transform for image denoising," *IET Image Process.*, vol. 5, no. 3, pp. 249–260, Apr. 2011.

[9] X. Yang, Y. Shi, L. Chen, and Z. Quan, "The lifting scheme for wavelet bi-frames: Theory, structure, and algorithm," *IEEE Trans. Image Process.*, vol. 19, no. 3, pp. 612–624, Mar. 2010.

[10] Y. Shi and X. Yang, "The lifting factorization of wavelet bi-frames with arbitrary generators," *Math. Comput. Simul.*, vol. 82, no. 4, pp. 570–589, Dec. 2011.

[11] Y. Shi and X. Yang, "The lifting factorization and construction of wavelet bi-frames with arbitrary generators and scaling," *IEEE Trans. Image Process.*, vol. 20, no. 9, pp. 1–11, Sep. 2011.

[12] A. L. da Cunha, J. Zhou, and M. N. Do, "The nonsubsampled contourlet transform: Theory, design, and applications," *IEEE Trans. Image Process.*, vol. 15, no. 10, pp. 3089–3101, Oct. 2006.

[13] M. S. Crouse, R. D. Nowak, and R. G. Baraniuk, "Wavelet-based statistical signal processing using hidden Markov models," *IEEE Trans. Image Process.*, vol. 46, no. 4, pp. 886–902, Apr. 1998.

[14] S. G. Chang, B. Yu, and M. Vetterli, "Adaptive wavelet thresholding for image denoising and compression," *IEEE Trans. Image Process.*, vol. 9, no. 9, pp. 1532–1546, Sep. 2000.

[15] J. Portilla, V. Strela, M. J. Wainwright, and E. P. Simoncelli, "Image denoising using scale mixtures of Gaussians in the wavelet domain," *IEEE Trans. Image Process.*, vol. 12, no. 11, pp. 1338–1351, Nov. 2003.

[16] I. W. Selesnick, "The estimation of Laplace random vectors in additive white Gaussian noise," *IEEE Trans. Image Process.*, vol. 56, no. 8, pp. 3482–3496, Aug. 2008.

[17] F. Shi and I.W. Selesnick, "An elliptically contoured exponential mixture model for wavelet based image denoising," *Appl. Comput. Harmon. Anal.*, vol. 23, no. 1, pp. 131–151, Jul. 2007.

[18] R. R. Coifman and D. L. Donoho, "Translation-invariant de-noising," in *Wavelets and Statistics*. New York, NY, USA: Springer-Verlag, 1995, pp. 125–150.

[19] M.Shim and A.Laine, "Overcomplete lifted wavele representations for multiscale feature analysis," in *Proc. ICIP*, Oct. 1998, pp. 242–246.

[20] M. Holschneider, R. Kronland-Martinet, J. Morlet, and P. Tchamitchian, "A real-time algorithm for signal analysis with the help of the wavelet transform," in *Wavelets. Time-Frequency Methods and Phase Space*. New York, NY, USA: Springer-Verlag, 1989, pp. 289 297.

[21] R. Eslami and H. Radha, "Translation-invarian contourlet transform and its application to image denoising," *IEEE*

Trans. Image Process., vol. 15, no. 11, pp. 3362–3374, Nov. 2006.
[22] I. Daubechies, B. Han, A. Ron, and Z. W. Shen, Framelets: MRAbased constructions of wavelet frames," *Appl. Comput. Harmon. Anal.*, vol. 14, no. 1, pp. 1–46, Jan. 2003.
[23] A. C. Bovik, M. Clark, and W. S. Geisler, "Multichannel texture analysis using localized spatial filters," IEEE Trans. Pattern Anal. Mach. Intell., vol. 12, no. 1, pp. 55–73, Jan. 1990.
[24] J.-K. Kamarainen, V. Kyrki, and H. Kälviäinen, "Invariance properties of Gabor filter-based features-overview and applications," *IEEE Trans. Image Process.*, vol. 15, no. 5, pp. 1088–1099, May 2006.
[25] J. P. Jones and L. A. Palmer, "An evaluation of the two-dimensional Gabor filter model of simple receptive fields in cat striate cortex," *J. Neurophysiol.*, vol. 58, no. 6, pp. 1233–1258, Dec. 1987.